Drosophila embryos spatially sort their nutrient stores to facilitate their utilization

Marcus D. Kilwein[1], Matthew R. Johnson[1#], Jonathon M. Thomalla[1&], Anthony Mahowald[2$], Michael A. Welte[1*]

[1] Department of Biology, University of Rochester, Rochester, NY
[2] Whitehead Institute for Biomedical Research, Cambridge, MA

Current addresses:
& Department of Molecular Biology and Genetics, 421 Biotechnology Building, Ithaca, NY 14850
# Department of Molecular Biology, Princeton University, Princeton, NJ 08544

$ 16 Barnard Rd., Belmont, MA 02478

* Corresponding author: Michael A. Welte, Department of Biology, RC Box 270211, 317 Hutchison Hall Rochester, NY 14627 USA, Tel (585) 276-3897, FAX (585)275-2070; e-mail: michael.welte@rochester.edu

Keyword(s): glycogen, lipid droplets, embryogenesis, developmental metabolism

Abstract

Animal embryos are provisioned by their mothers with a diverse nutrient supply critical for development. In Drosophila, the three most abundant nutrients (triglycerides, proteins, and glycogen) are sequestered in distinct storage structures, lipid droplets (LDs), yolk vesicles (YVs) and glycogen granules (GGs). Using transmission electron microscopy as well as live and fixed-sample fluorescence imaging, we find that all three storage structures are dispersed throughout the egg but are then spatially allocated to distinct tissues by gastrulation: LDs largely to the peripheral epithelium, YVs and GGs to the central yolk cell. To confound the embryo's ability to sort its nutrients, we employ mutants in Jabba and Mauve to generate LD:GG or LD:YV compound structures. In these mutants, LDs are missorted to the yolk cell and their turnover is delayed. Our observations demonstrate dramatic spatial nutrient sorting in early embryos and provide the first evidence for its functional importance.

Introduction

After fertilization, animal embryos develop for extended periods without access to external nutrients. In oviparous species, for example, the young animal gains access to additional nutrients only after hatching when it can feed independently. Therefore, mothers provision their embryos with nutrient reserves to enable embryonic development. In Drosophila, these reserves include neutral lipids (triglycerides and sterol esters), proteins (yolk proteins) and carbohydrates (predominantly glycogen)[1-4]. These nutrients provide both energy supplies and carbon backbones for anabolic metabolism. Different nutrients are not present freely in the cytoplasm, but are segregated from each other and packaged into distinct structures[5]. Neutral lipids are present in the center of lipid droplets (LDs), ubiquitous cellular organelles in which a single phospholipid layer surrounds a central hydrophobic core. Yolk proteins reside inside membranous yolk vesicles (YVs), oocyte- and embryo-specific LROs (lysosome-related organelles) delimited by a phospholipid bilayer. Glycogen forms so-called β particles (carbohydrate chains attached to the priming protein Glycogenin) that assemble into larger glycogen granules (GGs or α particles). These nutrients are utilized at different rates and at different embryonic stages[2,3,6,7]. Most previous studies relied on biochemical analysis of whole embryos and thus could not address the spatial organization of these nutrients in the embryo. In this paper, we address this issue and find that GGs, LDs, and YVs undergo dramatic sorting in the first few hours of embryogenesis and that this sorting is a prerequisite for proper nutrient utilization.

Drosophila embryos are a syncytium for the first ~2.5hrs. During this period, the nuclei divide 13 times near synchronously before undergoing bulk cytokinesis. The first 8 divisions (stage 1 and 2) occur deep within the embryo, with a minority of nuclei staying in the interior and most migrating to the periphery. Arrival of nuclei at the surface and formation of pole cells/germline (stage 3) mark the beginning of the syncytial blastoderm. Over the next hour (stage 4), the peripheral nuclei undergo the 9th-13th divisions[8]. Stage 5 encompasses a 1hr long interphase where a simultaneous cytokinesis (cellularization) generates ~6000 diploid cells organized as an epithelium at the embryo's periphery and one central, syncytial yolk cell. The epithelium gives rise to all the tissues of the future larva and adult, while the yolk cell is a transient tissue that functions as a yolk protein depot as well as a positional cue during the maturation of ecto- and endoderm[8,9]. Gastrulation movements (stage 6) and germ-band extension (stages 7-10) then transform this 2D epithelial layer into a complex 3D body plan.

The embryo initially shows little or no spatial segregation of nutrients, with LDs and YVs homogeneously distributed[10]. In larvae and adults, in contrast, nutrients are unevenly distributed, with specialized storage tissues dedicated to receiving and disseminating specific nutrients (*e.g.*, fat body tissue for fat storage). Nutritional specialization is already evident at gastrulation when LDs and YVs are allocated to distinct cells: most LDs to the peripheral epithelium; YVs exclusively to the yolk cell[11]. This distribution persists for the rest of embryogenesis (Fig. 1a-c). Thus, one of the first organizational events in Drosophila embryogenesis differentially sorts nutrients, foreshadowing nutrient handling by specialized tissues in later life stages.

79 How embryos spatially control the third major nutrient, glycogen, remains unknown. We
80 therefore visualized GGs using Periodic Acid-Schiff (PAS) staining and fluorescence microscopy
81 as well as a Glycogenin-YFP fusion. These approaches revealed GGs as highly dynamic,
82 undergoing both morphological changes and redistribution before cellularization. By
83 gastrulation, GGs are almost exclusively allocated to the yolk cell, like YVs. We also found that
84 in embryos lacking the LD protein Jabba, LDs are tightly associated with GGs and are
85 transported together to the yolk cell. These misallocated LDs are consumed slower than in the
86 wild type and persist through hatching. Perturbed LD turnover is likely the result of LD
87 misallocation, since delayed consumption is also observed in embryos in which LD
88 misdistribution results from inappropriate interactions with YVs. We conclude that early
89 nutrient sorting during Drosophila embryogenesis leads to an optimal nutrient allocation,
90 ensuring that nutrients are utilized efficiently.

91 **Results**

92 Lipid droplets and yolk vesicles are sorted to different tissues by cellularization

93 Previous studies had suggested that LDs and YVs are likely present throughout early Drosophila
94 embryos [11]. However, they had relied on fluorescence microscopy of whole mount samples. To
95 unambiguously determine the distribution of LDs and YVs, we analyzed the two organelles in
96 cross-sections using TEM. Both LDs and YVs were homogenously distributed throughout the
97 depth of the embryo (Fig. 1e; in the lower left, LDs are false colored in yellow, YVs in blue).
98 Thus, early embryos start out with LDs and YVs intermixed.

99 In stage 2 embryos, myosin-II mediated contractions of the cortex lead to large-scale circular
100 flows[12,13]. At the periphery, cytoplasm flows from the pole along the cortex to the middle of the
101 embryo where it descends towards the interior and then flows along the long axis of the
102 embryo to reemerge at the poles[12] (cartooned in Supplementary Fig. 3 f). YVs are known to be
103 carried by this flow[12]. We injected embryos with an LD-specific dye and monitored them live by
104 confocal microscopy (Video S1). In stage 2, LDs flow in the expected pulsative manner along the
105 periphery. In subcortical planes (Video S2), individual particles can be followed for long
106 distances, allowing us to quantify the flow of several organelles by particle image velocimetry[14]
107 (see below). Because our imaging conditions do not allow us to image the middle of the
108 embryo, we could not directly observe their flow in the embryo center. However, movies taken
109 at 40 µm depth (Video S1) are consistent with massive rearrangement of these interior LDs and
110 their flow towards the poles.

111 Previous fixed-embryo analysis had found that by Stage 3, LDs are highly enriched in the
112 peripheral ~40 µm of the embryo[10,15], while YVs remain throughout. We see the same pattern
113 in our movies, where LDs enrich at the periphery during Stage 2 and remain enriched there
114 through Stage 5 (Video S1). During Stage 4, YVs deplete from this region[13], and by stage 9, LDs
115 and YVs have segregated into the epithelial cells versus the yolk cell[11], respectively, a
116 distribution that remains through the rest of embryogenesis (Fig. 1b,c)[10,15].

117 In summary, YVs and LDs are intermixed in the early embryo and segregate from each other in
118 two steps. During stage 2, LDs enrich in the periphery, and during stage 4, YVs deplete from the
119 same region. As a result, the two nutrient stores are allocated to distinct cells by cellularization,
120 creating an early nutrient differentiation between the cells of the embryo (Fig. 1a).

121

122 Two novel, subcellular approaches to visualize glycogen granules by light microscopy

123 Does the third nutrient store (GGs) also undergo sorting? By electron microscopy, GGs appear
124 as large, weakly staining, membrane-less structures (Fig. 1f). TEM cross sections of young
125 embryos show that GGs are evenly distributed early on, like LDs and YVs (Fig. 1e, GGs in red in
126 the lower left). Thus, all three structures are present throughout the embryo at the start of
127 development.

128 To visualize GGs by light microscopy, we employed Periodic acid-Schiff (PAS) staining, a
129 histological stain for visualizing carbohydrates. This approach works well at the organismal and
130 tissue levels, but it does not reveal the subcellular organization into GGs. PAS-stained early

Figure 1

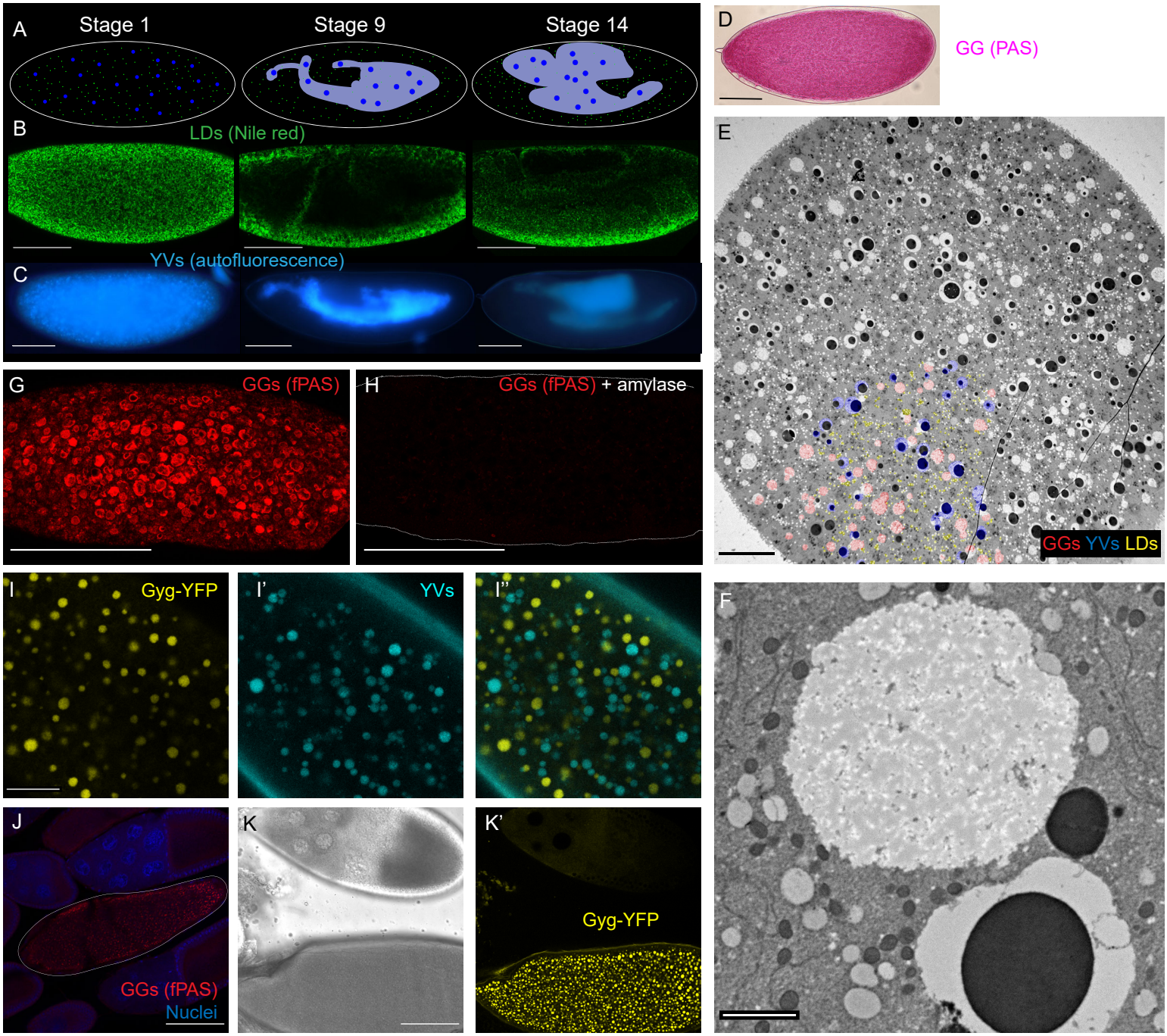

Ovaries

131 Figure 1. Visualizing embryonic nutrient stores. A,B,C) Distribution of LDs and YVs at three
132 embryonic stages (stage 1 = newly laid; stage ~ 4.5 hr old; stage ~ 11-hr old). A) Cartoon
133 summary, LDs are in green, YVs in blue, yolk cell in gray. B) Fixed embryos stained with Nile Red
134 to label LDs and imaged with confocal microscopy. Scale bar = 100 µm. C) Living embryos
135 imaged by epifluorescence microscopy to reveal the distribution of the autofluorescent YVs.
136 Scale bar = 100 µm. D) fPAS staining of newly laid embryo visualized by brightfield. Scale bar =
137 100 µm. E) Cross-section of a stage 1 embryo imaged by TEM; LDs, GGs, and YVs are evenly
138 distributed. A portion of the storage organelles are pseudo-colored, to orient the viewer, in the
139 lower left: YVs blue, LDs yellow, GGs red. Scale bar = 20 µm. F) TEM image of a GG, the large
140 white circle top/middle of the image. Scale bar = 2 µm. G,H) fPAS staining of newly laid embryos
141 visualized by confocal microscopy; the embryo in H was pretreated with α-amylase for 2hrs to
142 digest glycogen. Scale bars = 100 µm. I, I', I'') Confocal micrographs of a live stage 2 embryo
143 expressing Glycogenin-YFP. Scale bar = 20 µm. I = Glycogenin-YFP, I' = yolk autofluorescence, I''
144 = merged. J,K) Glycogen accumulation in ovary follicles; scale bar = 100 µm. J) PAS and DAPI
145 stained follicles, PAS signal is visible only in the stage 13 oocyte (outlined), with no signal in the
146 stage 10 follicle above it). K, K') Follicles expressing Glycogenin-YFP. K = bright field; K' = YFP
147 channel. GGs are not detectable at stage 10 (top) but are prominent in stage 14 (bottom).

148 embryos show signal throughout the cytoplasm, but conventional imaging approaches do not
149 reveal fine structure (Fig. 1d). However, when adapted for fluorescence microscopy (Thomas
150 Kornberg, personal communication), fluorescent PAS (fPAS) signal revealed discrete granular
151 structures of <1-5µm diameter throughout the cytoplasm (Fig. 1g). When embryos were
152 pretreated with α-amylase to degrade glycogen, fPAS signal was largely abolished (Fig. 1h),
153 confirming that most fPAS signal in the early embryo represents glycogen. As an independent
154 test, we analyzed fPAS signal during oogenesis, where glycogen specifically accumulates in late-
155 stage oocytes (Stage 13 and 14)[5,16]. fPAS signal recapitulates this pattern: only the oldest
156 oocytes were fPAS positive (Fig. 1j). We conclude that fluorescent imaging with PAS staining
157 labels glycogen, with sufficient contrast to resolve individual granules.

158 Live observation of YVs and LDs has revealed detailed information about their mechanism of
159 motion [11]. Because β particles, the subunits of GGs, contain the priming protein Glycogenin at
160 their center [17], we employed a protein trap line[18] in which an additional coding YFP exon is
161 inserted into the endogenous *Glycogenin* (*Gyg*) gene. By confocal microscopy, we observed
162 structures ~1-5 µm in diameter in stage 2 embryos of this strain (Fig. 1i). Because YFP
163 fluorescence is destroyed by PAS staining, we could not directly compare PAS-stained GGs and
164 Glycogenin-YFP, but several lines of evidence strongly support that Glycogenin-YFP indeed
165 reveals GGs. First, size, distribution, and abundance of the YFP-positive structures fit the GGs
166 visualized by PAS staining (Fig. 1g). Second, the only known abundant embryonic structures in
167 this size range are YVs and GGs, and live imaging of embryos revealed that the autofluorescent
168 YVs are distinct from the YFP structures (Fig. 1i,i',i''). Third, during oogenesis, YFP structures
169 become distinct only in Stage 13 and Stage 14 oocytes (Fig. 1k,k'), just like GGs (Fig. 1j). Fourth,
170 in certain mutants (see below), LDs are arranged around GGs (as observed by TEM or fPAS), and
171 we observe the same association around Glycogenin-YFP granules (Fig. 3g'). Thus, Glycogenin-
172 YFP reveals GGs.

173 As a final test, we performed *in-vivo* embryo centrifugation, a technique in which living
174 syncytial embryos are centrifuged to separate their components by density[19,20]. GGs as revealed
175 by PAS staining represent the densest fraction, opposite the low-density neutral lipid
176 (Supplementary Fig. 1b); this fraction appears clear in bright light (Supplementary Fig. 1a),
177 fitting a lipid free fraction. Similarly, in centrifuged Glycogenin-YFP embryos, YFP signal
178 accumulates at the very bottom of the embryos, even below the autofluorescent YVs
179 (Supplementary Fig. 1b). In centrifuged oocytes, coalesced GGs also form a cap below tightly
180 packed YVs[5].

181

182 <u>Glycogen distribution changes during development leading to yolk cell allocation</u>

183 By TEM, GGs are present throughout the embryo in stages 1 and 2, just like YVs and LDs (Fig.
184 1e). To determine whether GGs are also spatially sorted during embryogenesis, we performed
185 fPAS staining on embryos of different ages. In stage 1, glycogen was evenly distributed (Fig. 1G).
186 By stage 3, imaging in a subcortical plane shows a reduction in the number of GGs at the
187 embryo's surface (compare Fig. 2a to Fig. 1g). In stage 5, fPAS signal was absent from the
188 periphery; the embryo shown in Fig. 2B was imaged 40 µm below the surface (embryo is

Figure 2

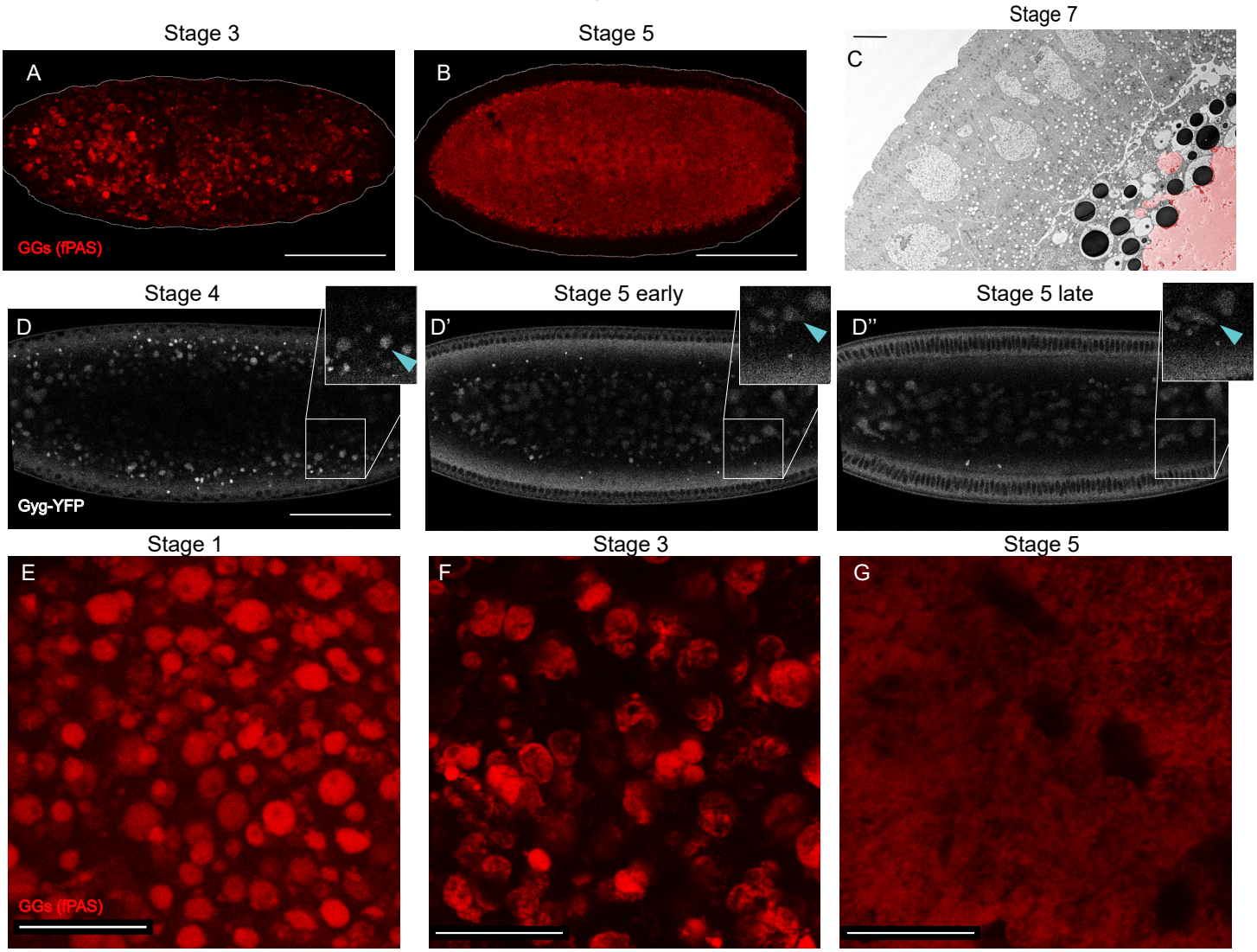
Stage 3
A
GGs (fPAS)
Stage 5
B
Stage 7
C
Stage 4
D
Gyg-YFP
Stage 5 early
D'
Stage 5 late
D''
Stage 1
E
GGs (fPAS)
Stage 3
F
Stage 5
G

189 Figure 2. GGs change their morphology and distribution during the first 3 hours of
190 embryogenesis. A,B) PAS staining of whole embryos, imaged by confocal microscopy. Scale bars
191 = 100 µm. A) Stage 3 embryo with GGs beginning to coalesce. B) Stage 5 embryo with coalesced
192 GGs localized to the embryo interior. C) TEM image of a stage 6 embryo; coalesced glycogen
193 (false colored red) evident in the yolk cell which occupies the bottom right corner, scale bar = 5
194 µm. D) Frames from confocal time-lapse movie of Glycogenin-YFP expressing embryo (Video
195 S4). Note the inward movement of the GGs and their coalescence. Scale bar = 100 µm. E, F, G)
196 fPAS staining of embryos of different stages; scale bar = 20 µm. The reduced signal in (G) is
197 likely a result of the deeper focal plane due to inward motion of the GGs.

198 outlined in white). This developmental time course suggests that GGs deplete from the
199 peripheral regions.

200 Live imaging of Glycogenin-YFP expressing embryos identified discrete, mobile GGs in young
201 embryos (Video S2). Fig.2 d-d" shows still images from a movie (Video S3) for an embryo
202 imaged ~40 µm below the surface through stages 4 to 5. Initially (Fig. 2d), GGs were enriched in
203 a broad area just below the peripheral nuclei (black circles). Over time, GGs progressively
204 moved into the interior. By the onset of stage 5 (Fig. 2d'), GGs were largely absent from this
205 area and most were in the center. Towards the end of stage 5, the GGs were deep within the
206 embryo's interior (Fig. 2d''), well below the forming cells. This inward movement was confirmed
207 using epifluorescence microscopy (Supplementary Fig. 2a).

208 Thus, both fPAS and live imaging show redistribution of GGs into the embryo's interior during
209 stages 3-5. This pattern suggests that after cellularization the GGs are allocated to the yolk cell
210 and are absent from the surrounding epithelium. This distribution was confirmed by TEM
211 imaging: the stage 7 embryo in Fig. 2c has glycogen (false colored in red) entirely in the yolk cell
212 (see also Fig. 4b). And fPAS staining of embryos in stages 9 and 10 reveals that the majority of
213 glycogen is indeed in the yolk cell (Supplementary Fig. 2b). Overall signal is much reduced at
214 that time, and by stage 11 we can no longer detect appreciable fPAS signal (Supplementary Fig.
215 2c), suggesting that glycogen is being turned over. Glycogenin-YFP is also restricted to the yolk
216 cell in later stages (Supplementary Fig. 2c).

217

218 <u>GG morphology changes during development</u>

219 Our fPAS and Glycogenin-YFP time courses suggest that GG morphology changes as the embryo
220 develops. We therefore examined fPAS-stained embryos at higher magnification. Newly laid
221 embryos were characterized by discrete GGs evenly distributed within the focal plane (Fig. 2e).
222 In Stage 3, GGs were arranged much less homogeneously, forming clusters: frequently, multiple
223 GGs were in close contact with each other, and there was glycogen-free space between clusters
224 (Fig. 2f). This pattern implies that GGs not only move inwards (*i.e.,* perpendicular to the focal
225 plane shown), but also within the plane towards each other. Consistent with that notion, some
226 of the GGs are no longer round, but appear as oblong or more complicated aggregates,
227 implying that GGs are coalescing. By stage 5, fPAS signal forms a single, largely homogeneous
228 mass (Fig. 2g) that only retains remnants of the granular structure at its outer edges (Fig. 2c).
229 This single GG mass occupies the center of the embryo (Fig. 2b). Consistently, TEM imaging of
230 stage 7 embryos reveals a large, fused glycogen structure (Fig. 2c, red colored area).

231 We observed this same morphology shift in movies of Glycogenin-YFP embryos (Fig. 2d-d";
232 Video S3; Supplementary Fig. 2a). In stage 4, GGs near the periphery are largely discrete
233 structures, while GGs deeper in the embryo tend to be larger and are misshapen, consistent
234 with fusion. Over time, as the GGs shifted towards the embryos center, they formed larger, less
235 spherical entities (stage 5 early, Fig. 2d'; Supplementary Fig. 2a), so that by stage 5's end, GG
236 signal showed many amorphous structures in the embryo's interior (Fig. 2d''; Supplementary
237 Fig. 2a). The insets in Fig. 2d-d'' track a single GG indicated with a blue arrowhead as it moved

238 inward and closer to other GGs and then fused. In summary, GGs undergo a dramatic
239 morphological shift as they migrate into the center of the embryo.

240

241 Lack of the LD protein Jabba results in tight association between LDs and GGs

242 Our analysis shows that LDs, GGs, and YVs are initially intermixed but are segregated to distinct
243 tissues by cellularization: while most LDs end up in the peripheral epithelium, both YVs and GGs
244 are allocated to the interior yolk cell. The enrichment of both protein and glycogen stores in the
245 yolk cell is consistent with the idea of the yolk cell as a metabolically supportive tissues[8,9,21]. But
246 why LDs are allocated differently and why the embryonic nutrient supply is spatially organized
247 at all is unknown.

248 As a potential inroad into this problem, we re-examined embryos lacking the LD protein Jabba,
249 one of the most abundant proteins on embryonic LDs[22]. Such embryos have normal triglyceride
250 content but display abnormal LD distribution in stage 4[22]. When we imaged fixed stage 1-2
251 embryos stained for LDs, wild-type embryos displayed the pattern expected from our TEM
252 analysis (Fig 1e); LDs were absent from many circular areas (presumably GGs and YVs) but
253 distributed evenly throughout the remaining spaces (Fig. 3a). The pattern in *Jabba* mutants
254 (two different alleles, $Jabba^{DL}$ and $Jabba^{zl01}$) was dramatically different. Here most LDs were
255 accumulated in rings, with few LDs occupying the space between the rings (Fig. 3b, and data
256 not shown). This aberrant distribution was not an artefact of fixation, as we saw the same
257 pattern in embryos injected with LD dyes and imaged live (Supplementary Fig. 3d, 0s panel).

258 The pattern in *Jabba* mutants suggests that LDs accumulate around YVs or GGs. Co-detection of
259 LDs and YVs revealed no association between them (Supplementary Fig. 3e). In contrast, co-
260 labeling of GGs and LDs showed that LDs were surrounding GGs (Fig. 3A'-B"). This finding was
261 further confirmed in TEM cross sections (Supplementary Fig 4A). A similar, but less pronounced
262 association was already observed when *Jabba* dosage was reduced (Supplementary Fig. 3c *1x*
263 *Jabba*). We employed this observation to confirm LD-GG association in living embryos. We
264 injected LipidSpot610 into embryos from mothers expressing Glycogenin-YFP and either one or
265 two copies of the wild-type *Jabba* gene. LDs and GGs displayed minimal association in the
266 otherwise wild-type background (Fig. 3g), while many LDs were present at or near the surface
267 of GGs when *Jabba* dosage was reduced (Fig. 3g'). We conclude that when Jabba levels are
268 reduced, LDs associate with GGs. This association can already be observed in oocytes, as soon
269 as GGs are detected (Fig. 3e-f'). Finally, we detected no association between LDs and GGs when
270 other LD proteins are missing, namely PLIN-2/LSD-2, Sturkopf/CG9186, or Klar (Supplementary
271 Fig. 3c). We conclude that Jabba uniquely suppresses inappropriate interactions between these
272 storage structures.

273 Although we occasionally observe LDs deep within GGs of *Jabba* mutants, for the most part the
274 LDs are arranged in a ring pattern with glycogen in the center (Fig. 3d"). In fact, LDs appear
275 embedded within the outer regions of the GGs; see, for example, Fig. 3d',d", where GGs display
276 indentations/areas of exclusion in the PAS signal (Fig. 3d', arrowheads). These regions are filled
277 with LDs (Fig. 3d"). Rarely were such associations or indentations observed in wild type (Fig. 3c',
278 arrowheads). TEM confirmed a tight LD-GG association: in *Jabba* embryos, LDs appear to

Figure 3

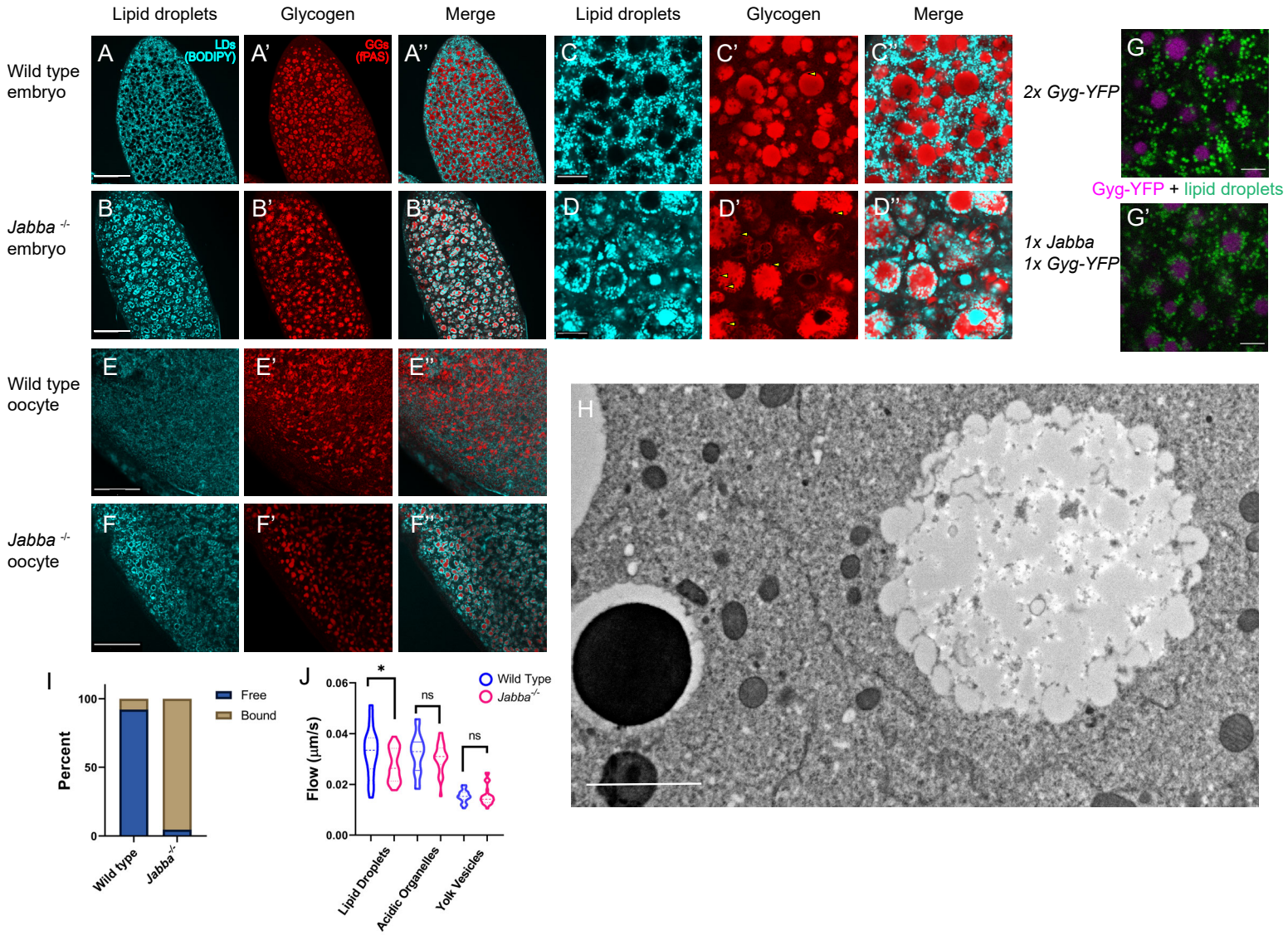
Lipid droplets
Glycogen
Merge
Lipid droplets
Glycogen
Merge
Wild type embryo
Jabba -/- embryo
Wild type oocyte
Jabba -/- oocyte
LDs (BODIPY)
GGs (fPAS)
2x Gyg-YFP
1x Jabba
1x Gyg-YFP
Gyg-YFP + lipid droplets
Free
Bound
Percent
Wild type
Jabba-/-
Wild Type
Jabba-/-
Flow (µm/s)
Lipid Droplets
Acidic Organelles
Yolk Vesicles
ns

Figure 3. LDs and GGs aberrantly interact in *Jabba* mutant embryos. A-F'') LDs (cyan, BODIPY) and GGs (fPAS, red). A-B'') Stage 2 embryos; scale bars = 60 µm. A-A'') wild type, B-B'') *Jabba*. C-D'') the same embryos at a higher magnification. Scale bars = 10 µm. Arrowheads (C'&D') indicate indentations in GGs occupied by LDs. E-F'') Late-stage oocytes stained for LDs (cyan, BODIPY) and GGs (fPAS, red). Scale bars = 40 µm. GG-LD association is already visible in F''. G,G') LDs (green, LipidSpot610) and GGs (magenta, Glycogenin-YFP) in Glycogenin-YFP (G) and 1 x Glycogenin-YFP,1 x *Jabba* (G') embryos. 1x *Jabba* embryos display LD-GG association not found in the wild type. Scale bars = 5 µm. H) TEM image of *Jabba* embryo; GG with its surface decorated by bound LDs. LDs are largely absent from the cytoplasm. Scale bar = 2 µm. I) quantification of the number of LDs bound to GGs vs free in wild-type and *Jabba* embryos. Quantitation of 3 TEM images per genotype (>400 LDs) revealed that the majority of LDs are not associated with GGs in the wild type, while ~95% of LDs are bound to GGs in *Jabba* embryos. J) PIV analysis of motion of LDs, lysosomes (acidic organelles), and YVs in wild-type and *Jabba* embryos. The variation in speeds for a given organelle results from the pulses at the embryo's cortex. Mean LD velocity in wild type versus *Jabba*: 0.034 vs. 0.028 µm/s; $p = 0.0144$. Mean velocity of acidic organelles: 0.032 vs 0.031 µm/s, $p = 0.406$. Mean velocity of YVs: 0.015 vs 0.016 µm/s, $p = 0.815$. Analysis based on at least 3 embryos per genotype, with 9 measurements per embryo, i.e., n values of at least 27. p-values generated by unpaired, two tailed t-tests. * $p<0.05$.

298 directly contact GGs, with glycogen bulging out between LDs (Fig. 3h; Supplementary Fig. 3b). In
299 the wild type, such association is observed rarely (Fig. 1e; Supplementary Fig. 3a; Fig. 3i). This
300 association is strong enough that when *Jabba* embryos are centrifuged, the dramatic separation
301 of LDs and GGs into distinct layers at opposite ends of the embryo observed in the wild type
302 (Supplementary Fig. 1b) is disrupted. In the *Jabba* mutant, glycogen signal is found intermixed
303 with the LD layer in the region of lowest density, and pockets of LD signal are present within the
304 glycogen layer in the highest-density region (Supplementary Fig. 1c).

305

306 Consequences of LD:GG interactions on LD motility

307 To determine if the LD/GG association in *Jabba* embryos affects LD motility, we labeled LDs by
308 injecting dyes into embryos, monitored their behavior live, and quantified their flow speeds by
309 particle image velocimetry[14]. In the wild type, LDs and acidic organelles flow faster than YVs
310 (Fig. 3j), presumably due to their smaller size. *Jabba* mutant embryos displayed the expected
311 ring-arrangement of LDs (Supplementary Fig. 3d); these rings moved as a unit (Video S5),
312 reinforcing that LD:GG complexes are stable structures. Compared to wild type, they displayed
313 stuttered motion, minimal displacement (Supplementary Fig. 3d), and lower average velocity
314 (Fig. 3j). In contrast, YVs and acidic organelles showed similar mobility between the two
315 genotypes (Fig. 3j). Thus, altered LD flow in *Jabba* embryos does not represent a general defect
316 in cytoplasmic streaming, but rather a specific disruption of LD motility, likely due to the much
317 larger size of LD:GG complexes relative to individual LDs.

318

319 Consequences of LD-GG interactions on LD allocation

320 During wild-type development, GGs and LDs are initially intermixed and homogeneously
321 distributed throughout the embryo (Fig. 1e, Supplementary Fig. 4a). LDs enrich at the periphery
322 by stage 3 (Video S1), and by the end of stage 5, GGs and LDs are segregated from each other
323 and allocated to different tissues. In the absence of Jabba, GGs and LDs form large composite
324 structures that are also distributed throughout the early embryo (Supplementary Fig. 4B). But
325 because these composite structures travel together, segregation to distinct locations seems no
326 longer possible. Indeed, in our movies with labelled LDs (Video S5, S6), the LDs trapped in
327 GG:LDs complexes were far less mobile, engaging in delayed, stuttered motion and did not
328 enrich in the periphery as in the wild type (Video S1). For post-cellularization embryos, TEM
329 analysis revealed a massive redistribution of LDs in *Jabba* embryos relative to wild type (Fig. 4b-
330 e), with fewer LDs in the peripheral epithelium and more in the yolk cell. In the wild type, 72%
331 of 510 LDs scored were present in the epithelial cells, while in *Jabba* embryos it was only 23% of
332 the 696 LDs scored.

333 In contrast, we only found minor differences in glycogen distribution between the two
334 genotypes. By fPAS staining, wild type and *Jabba* were very similar (Supplementary Fig. 2E). By
335 TEM, the bulk of GGs in *Jabba* embryos were appropriately localized to the yolk cell, just like in
336 the wild type (Fig. 4B-E). There were a few instances of small LD:GG complexes segregated into
337 blastoderm cells (Fig. 4E green arrowhead). We conclude that the composite LD-GG structures
338 in *Jabba* embryos are allocated like GGs, leading to LD mislocalization.

Figure 4

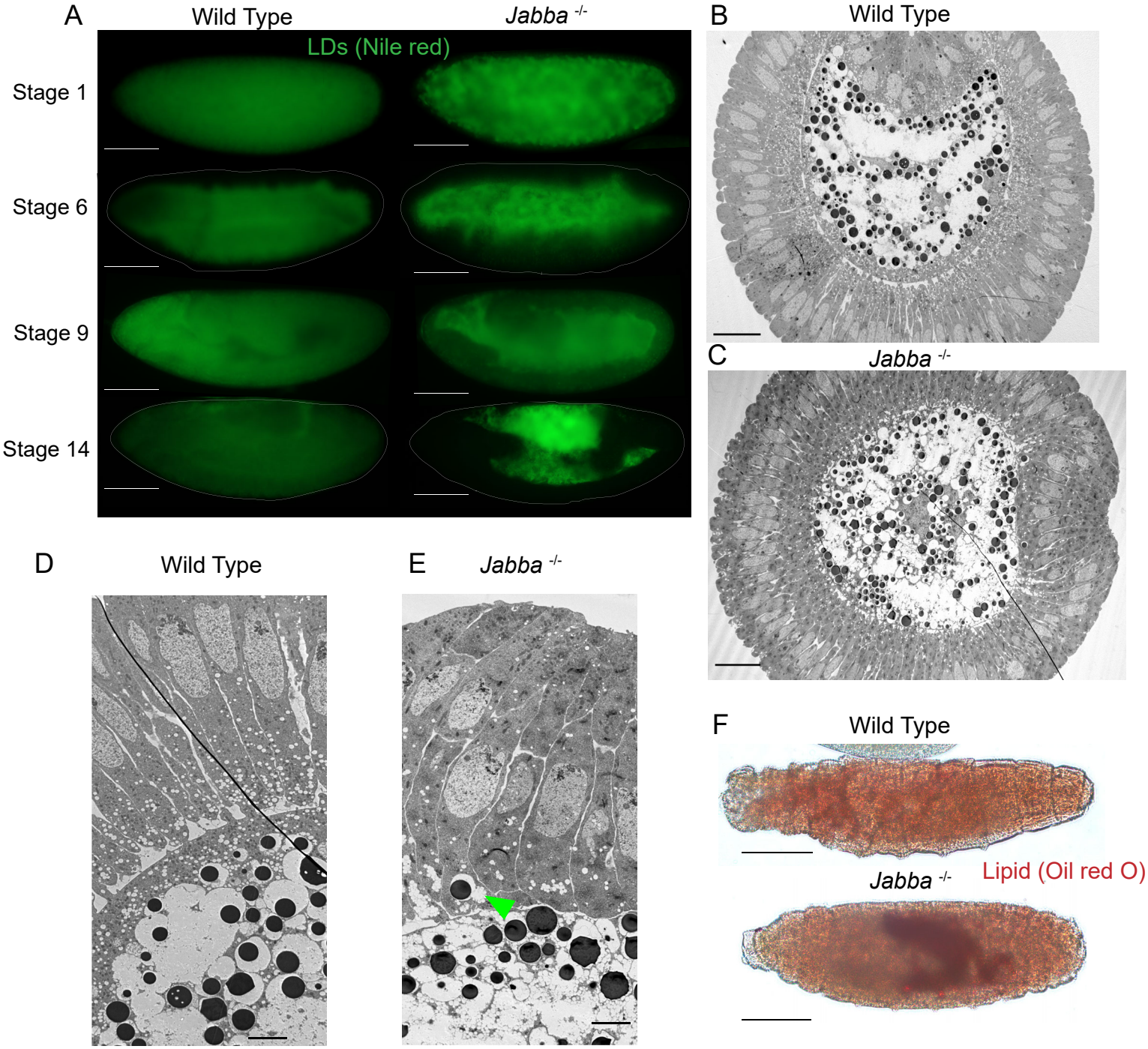
A
Wild Type
Jabba -/-
LDs (Nile red)
Stage 1
Stage 6
Stage 9
Stage 14
B
Wild Type
C
Jabba -/-
D
Wild Type
E
Jabba -/-
F
Wild Type
Jabba -/-
Lipid (Oil red O)

339 Figure 4. In *Jabba* mutant embryos, lipid droplets are mislocalized and their consumption is
340 disrupted. A) Wild-type and *Jabba* embryos of various stages stained with Nile red to detect LDs
341 and imaged with epifluorescence microscopy. Scale bars = 100 µm. B,C) TEM cross sections of
342 stage 6 embryos. B) ventral furrow is at the top of the image. C) the ventral furrow is at the
343 right of the image. Scale bars = 100 µm. D,E) TEMs of stage 6 embryos at higher magnification
344 showing the border between the cellularized epithelium (right) and yolk cell (left). Scale bars =
345 5 µm. The green arrowhead (E) shows a YV attached to LD:GG complex which has
346 inappropriately localized to the epithelium. F,G) L1 larva stained with Oil Red O to detect LDs.
347 Scale bar = 80 µm. The *Jabba* larva's residual LDs are visible in its gut.

348 As an independent approach, we detected LDs by Nile red staining and fluorescence microscopy
349 in whole-mount embryos (Fig. 4a). Already in early stages, LD distribution looks different: signal
350 is diffuse throughout the embryo for wild type and granular in *Jabba* mutants, presumably
351 reflecting LD enrichment around GGs. At the beginning of gastrulation, signal in the mutant is
352 more prominent in the yolk cell, a pattern that becomes even more pronounced in later stages.
353 By stage 14, LD signal is absent from the yolk cell and present everywhere else, while in *Jabba*
354 embryos this pattern is reversed (Fig. 4A). We conclude that in *Jabba* embryos the bulk of LDs
355 are indeed mislocalized to the yolk cell.

356 In late-stage embryos, LD signal in *Jabba* embryos was not only restricted to the yolk cell but
357 also displayed increased intensity. This difference even persisted post-hatching. LD staining
358 using Oil Red O revealed strong signal in the gut lumen (the location of the yolk cell remnant) of
359 newly hatched *Jabba* larvae (Fig. 4f), unlike wild type (Fig. 4f). Thus, *Jabba* mutants not only
360 mislocalize their LDs, but fail to consume them properly.

361

362 <u>LD interactions with YVs also lead to their mislocalization and persistence</u>

363 LD consumption in the mutant might be impaired because Jabba is important for LD breakdown
364 or because the yolk cell is not equipped to metabolize this high concentration of LDs. To
365 distinguish between these possibilities, we took advantage of a recent report that embryos
366 lacking the Mauve protein display an interaction between LDs and YVs[23]. Mauve is a resident
367 protein on lysosome related organelles (LROs) important for their maturation. YVs are a type of
368 LRO and in the absence of Mauve display several phenotypes, including an association with LDs
369 [23]. Might these YV-LD interactions affect nutrient sorting?

370 As strong disruption of Mauve severely impairs early embryonic development[23], we generated
371 mothers transheterozygous for two weak alleles, *mauve*^{Rosario} and *mauve*^{3}. These embryos
372 displayed LDs association with YVs (Fig. 5a arrow), as well as the YV size heterogeneity and
373 autofluorescence variability reported for stronger allele combinations (Fig. 5a)[23], but no obvious
374 association between GGs and LDs (Fig. 5b)[23].

375 The *mauve*$^{Rosario/3}$ YV-LD association was an exciting opportunity to test our model that LDs are
376 missorted during cellularization if they are associated with a structure destined for yolk cell
377 deposition, allowing us to utilize YVs instead of GGs. When the mutant embryos were stained
378 for LDs (Fig. 5c), signal in stage 1 was clustered instead of diffuse like in wild type (Fig. 4a). At
379 stage 9, LDs signal was predominately in the yolk cell, but also present in the other tissues (Fig.
380 5c). At stage 14, LD staining was clearly enriched in the yolk cell (Fig. 5a) relative to wild type
381 (Fig. 4a). Thus, mutations in two unrelated genes, *Jabba* and *mauve*, show that when LDs
382 inappropriately interact with other nutrient structures, they are mislocalized to the yolk cell and
383 are turned over more slowly.

Figure 5

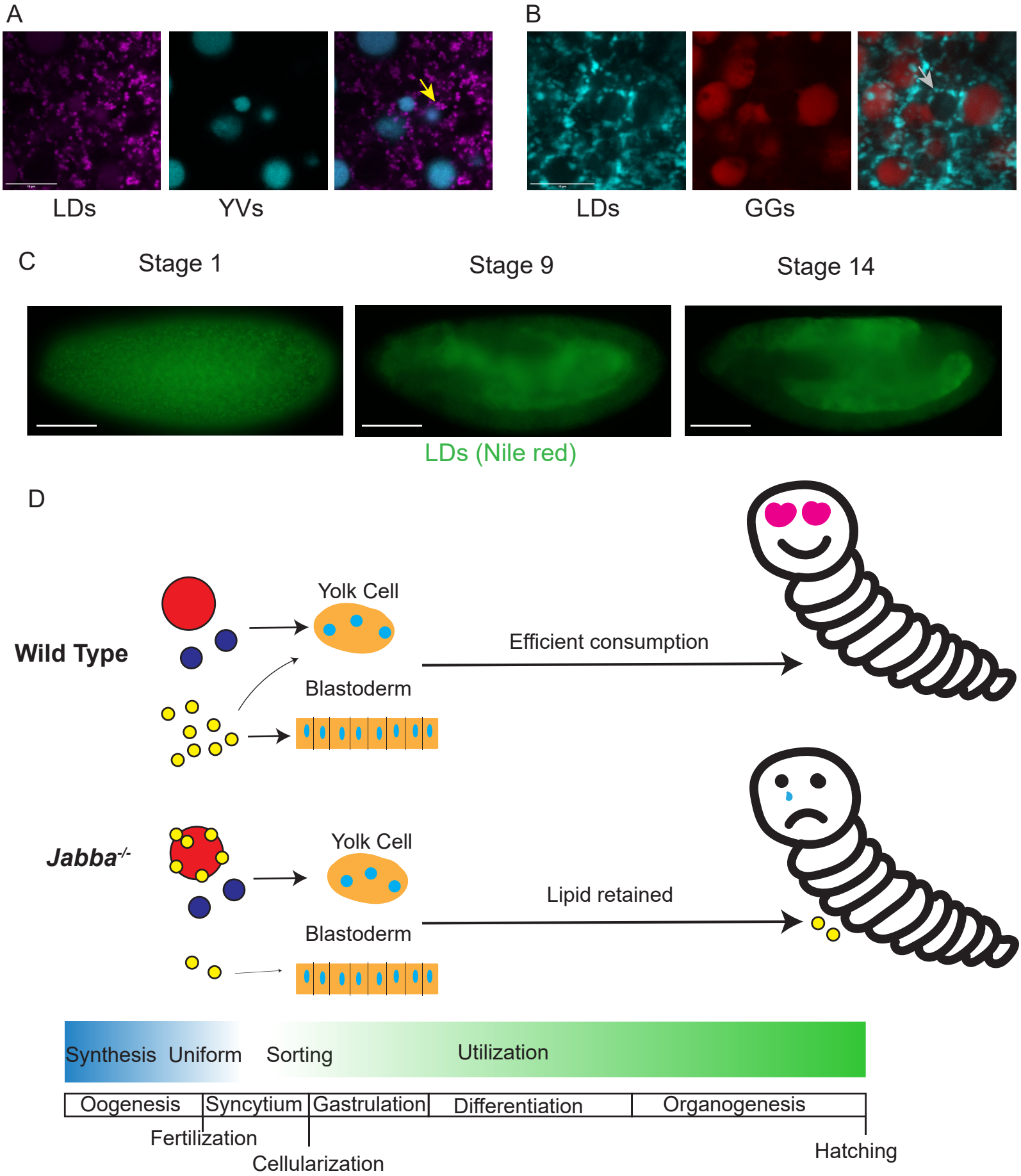
A
LDs
YVs
B
LDs
GGs
C
Stage 1
Stage 9
Stage 14
LDs (Nile red)
D
Wild Type
Yolk Cell
Blastoderm
Efficient consumption
Jabba-/-
Yolk Cell
Blastoderm
Lipid retained
Synthesis
Uniform
Sorting
Utilization
Oogenesis
Syncytium
Gastrulation
Differentiation
Organogenesis
Fertilization
Cellularization
Hatching

384 Figure 5. Disrupting LD localization disrupts LD consumption. A) Live imaging of LDs (magenta,
385 Lipid Spot 610) and YVs (blue, autofluorescence) in newly laid *mauve* mutant embryos. LDs are
386 associating adjacent to YVs. Note that the autofluorescence signal may not extend to the
387 furthest edges of the YV due to the double membrane structure of YVs. B) Fixed imaging of LDs
388 (blue, BODIPY) and GGs (red, fPAS) in *mauve* embryos. Arrow indicates rare LD ring not
389 associated with fPAS signal. We believe that this likely represents LDs around YVs with
390 undetectable autofluorescence. A,B) Confocal microscopy; scale bar = 10 µm. C) LD (green, Nile
391 red) distribution in fixed *mauve* embryos. Stage 1: LD clustering, presumably around YVs,
392 reminiscent of GG:LD cluster seen in *Jabba* mutants. Stage 9 and 14: mislocalization of LDs to
393 the yolk cell. Images by epifluorescence microscopy; scale bars = 100 µm. D) Model: nutrient
394 sorting from oogenesis through embryogenesis, comparing wild type with the disruptions seen
395 in *Jabba* mutants. Note that the timeline is not scaled to absolute developmental time but is
396 meant to show the brief life of nutrients through synthesis, distribution and consumption when
397 compared to other developmental events. Mislocalized LDs in *Jabba* mutants are speculated to
398 negatively affect completion of embryogenesis or the larvae itself.

399

400 **Discussion**

401 Glycogen is a major energy store in animals, uniquely capable of providing energy rapidly, both
402 aerobically and anaerobically. While glycogen's functions are well investigated in adult tissues,
403 its role during embryogenesis is less understood. In this study, we developed new tools to
404 determine the spatial distribution of glycogen in Drosophila oocytes and embryos. Consistent
405 with previous biochemical and electron microscopic analysis, we find that glycogen stores
406 accumulate late in oogenesis and are organized into large, membrane-less structures. These
407 GGs are evenly distributed throughout the early embryo and undergo two types of transitions
408 during syncytial stages. First, they are displaced from the subcortical region during stage 4,
409 leading to their accumulation in the center and allocation to the yolk cell. Second,
410 simultaneously, GGs fuse into larger and larger structures, so that by the end of stage 5, most
411 glycogen is present in a large superstructure in the yolk cell. LDs and YVs also start out with an
412 even distribution and are then specifically allocated. After stage 5, YVs are restricted to the yolk
413 cell, like GGs, while LDs are predominately sorted to the peripheral epithelial cells. In two
414 different mutant conditions, we find physical interactions between LDs and either GGs or YVs.
415 In both cases, LDs are misallocated to the yolk cell. In *Jabba* mutants, a portion of these LDs fail
416 to be consumed during embryogenesis and persist into larval stages; in *mauve* mutants
417 persistence through embryogenesis is milder, consistent with less severe mislocalization of LDs.
418 We conclude that mislocalizing LDs early in embryogenesis affects subsequent LD consumption.

419 GGs in Drosophila oocytes and embryos are akin to the α particles that mediate long-term
420 glycogen storage in many tissues, including muscle, liver, and fat body[17,24]. Their large size
421 (which must correspond to thousands of β particles[5] as opposed to ~30 in liver[24]) likely protects
422 against glycogen breakdown and facilitates their physical movement for differential allocation.
423 How α particles assemble and disassemble remains unclear. Proposed binding agents holding
424 neighboring β particles together include covalent links between glycogen chains[25,26] or
425 Glycogenin molecules at the surface of the β particles[27], in addition to the Glycogenin dimer in
426 their cores. We speculate that the amorphous mass of glycogen in stage 5 embryos represents
427 partial dissolution of GGs into β particles, as a prelude to enzymatic breakdown of glycogen.
428 Consistent with this notion, fPAS staining in stages 9-10 becomes very weak (Supplementary
429 Fig. 2b,c) and biochemical measures of glycogen levels show the same drop[2]. This timing for
430 glycogen depletion overlaps with a proposed switch in embryonic metabolism from
431 carbohydrate-based to triglyceride-based energy production[2]. Disassembly into β particles
432 might provide enhanced access for the cytosolic glycogen phosphorylase, responsible for most
433 glycogen turnover in embryos[28].

434 Going forward, Drosophila oocytes and embryos should be a powerful model for unraveling the
435 mechanism of the conversion between α and β particles. GGs are large enough to be followed
436 by light microscopy, their assembly and disassembly occurs quickly (within ~2hrs or less), and
437 Glycogenin-YFP allows live imaging of these processes. In fact, to our knowledge this is the first
438 example of live imaging of glycogen in any system.

439 Although during oogenesis the three major nutrient stores are made at different at times and
440 through different mechanisms[5,11], they all start out intermixed and homogenously distributed in
441 the early embryo. Nutrient sorting starts in stage 2 when myosin-II driven cortex contractions

442 establish large-scale cytoplasmic flows throughout the embryo. Flow speeds, as estimated from
443 the behavior of YVs, are sufficient to spread out the interior nuclei along the entire anterior-
444 posterior axis[12]. As LDs flow faster than YVs (Fig. 3j), these flows should be able to transport
445 most LDs from the center to the poles. If these LDs are somehow captured at the periphery,
446 reducing their return to the embryo center, it explains their enrichment in the periphery by
447 stage 3. Consistent with an important contribution from cytoplasmic flow, the LD-GG
448 aggregates in *Jabba* mutants flow with reduced speeds and LDs fail to enrich at the embryo
449 surface (Video S4). Thus, we propose that this cytoplasmic flow promotes the first step of
450 nutrient sorting, when LDs accumulate peripherally.

451 By stage 4 and 5, the nuclei at the embryo surface set up an array of radially oriented
452 microtubules that traverse a ~40 µm peripheral zone[10]. These microtubules are proposed to
453 push YVs into the interior [13], and GGs may be displaced by the same mechanism, as they
454 deplete from this zone at the same time. LDs, in contrast, move bidirectionally along these
455 microtubules, employing cytoplasmic dynein and kinesin-1[29,30]; this motion confines them to
456 the microtubule zone[15]. We propose that MTs keep LDs in the peripheral zone, while they push
457 GGs and YVs inward, resulting in the second sorting step. Our analysis of *Jabba* and *mauve*
458 mutants reveals that successful sorting also requires nutrient stores stay separated. When LDs
459 are tightly associated with either GGs or YVs, sorting fails, and LDs are misallocated to the yolk
460 cell.

461 Presumably the nutrients stored in GGs, YVs, and LDs all support the metabolic needs of the
462 developing embryo. Why then are they allocated differently? One reason might be the different
463 properties of their breakdown products. YVs' amino acids and GGs' glucose are water soluble,
464 making diffusion through gap junctions or membrane transporters viable options for
465 dissemination. Thus, the yolk cell can serve as a hub for glucose and amino acid distribution, as
466 it remains connected via cytoplasmic bridges to the blastoderm through stage 9[21,31] and
467 expresses numerous nutrient transporters. In contrast, free fatty acids (FAs) generated from LD
468 breakdown are poorly water-soluble and potentially toxic[32,33]; they are typically immediately
469 channeled into specific intracellular pathways[34]. For example, efficient FA transfer from LDs to
470 mitochondria requires proximity and direct contact[35-37]. Thus, allocation of LDs predominately
471 to the periphery would allow efficient local energy production. Intriguingly, during zebrafish
472 embryogenesis, LDs are initially highly enriched in the future yolk sac but are imported into the
473 embryo proper via cytoplasmic bridges and actin-myosin based motility[38,39]. Thus, the zebrafish
474 embryo may also depend on a local LD supply to support its dividing cells.

475 What are the consequences of mislocalizing LDs to the yolk cell? Our data indicate that a
476 fraction of these LDs persist through the end of embryogenesis. Although *Jabba* mutant
477 embryos are viable[22], their progression through embryogenesis has not yet been analyzed in
478 detail. Recent work on embryonic glycogen metabolism suggests that even minor disruption of
479 LD metabolism has the potential for widespread effects on embryogenesis. Embryos that either
480 lack glycogen reserves or are unable to access them display widespread changes in their
481 metabolome as well as hatching delays[28]. Since fat contributes roughly 10x the energy of
482 glucose (derived from glycogen) during Drosophila embryogenesis[3], even the modest retention
483 of LDs in *Jabba* mutants might have prominent effects on development.

484 LDs and GGs co-exist not only in embryos, but also in mature tissues (*e.g.*, muscle, intestinal
485 epithelia, liver, fat body)[17,40,41]. It is conceivable that in embryos inappropriate interactions
486 between LDs and GGs are particularly harmful because of the large size of GGs and the
487 extensive cytoplasmic streaming which presumably leads to many encounters between these
488 organelles. It will therefore be interesting if mechanisms to keep LDs and GGs apart are specific
489 to embryos or also important in other cells.

490 By devising novel imaging methods for glycogen storage structures, we have shown that
491 Drosophila embryos dramatically reorganize their nutrients by cellularization, with distinct
492 nutrients sorted into separate nascent tissues. The embryo employs multiple mechanisms to
493 get its nutrient stores to the correct location, including cytoplasmic streaming, preventing
494 inappropriate interactions, and microtubule-dependent transport. We also provide the first
495 evidence that correct spatial allocation of LDs is necessary for their efficient consumption.
496 Together, these observations suggest that embryos need to achieve an optimal nutrient
497 allocation to support subsequent steps in development (cartooned in Fig 5d) and that the
498 spatial allocation of nutrients is essential to fully understand embryonic metabolism. The
499 importance of this allocation is particularly remarkable as these nutrient stores only exist
500 transiently and are consumed by the end of embryogenesis.

501 **Methods**

502 Origin of fly strains

503 Oregon R was used as the wild-type strain. *Jabba*^{DL} and *Jabba*^{zl01} were generated previously in
504 the lab and are strong loss-of-function alleles with no Jabba protein detected in early
505 embryos[22]. *Df(2R)Exel7158/CyO* carries a large deletion that encompasses *Jabba* and is used to
506 reduce *Jabba* dosage; for simplicity, embryos from mothers carrying this deletion are referred
507 to as *1x Jabba*. This stock was obtained from the Bloomington *Drosophila* Stock Center (BDSC:
508 7895; FLYB: FBab0038053)]. The hypomorphic alleles *mauve*^{3} and *mauve*^{Rosario} (described in[23])
509 were a gift from Ramona Lattao. The YFP insertion in the Glycogenin locus was generated in a
510 large genetic screen[18] and was obtained from the Kyoto stock center (DGRC # 115562).

511

512 Microscopy

513 Laser scanning confocal microscopy was performed on a Leica SP5 equipped with HyD
514 detectors, using either a 40x objective to show most of the embryo, or a 63x objective for
515 subregions. Epifluorescence imaging was performed on a Nikon Eclipse E600 using a 20x
516 objective. All images were assembled in Adobe Illustrator.

517 Videos, except for Supplementary Video 4, were captured at 1 frame per 30 second and are
518 displayed at 20 frames per second. Supplementary Video 4 was captured at 1 frame per 15
519 minutes and displayed at 1 frame per 0.8 seconds. The orientation of the embryo was chosen to
520 maximize the amount of the embryo captured in frame. Video processing was performed in FIJI
521 (NIH).

522 Sample sizes were determined as follows. For live imaging, at least three embryos were imaged
523 per genotype per experiment. For fixed samples, the stainings were performed at least twice.
524 For TEM analysis, the core facility was given ten appropriately staged embryos per genotype
525 per experiment, and then chose which were imaged based on staining success.

526 Exclusion criteria for imaging embryos were predetermined. Embryos not of the stage of
527 interest, determined to have expired during preparation or image acquisition, or which were
528 imaged in the incorrect orientation/focal depth were excluded.

529

530 Periodic acid Schiff (PAS) and LD staining

531 Embryos were collected on apple juice plates for the desired time range and dechorionated
532 with 50% bleach and fixed for 20 min using a 1:1 mixture of heptane and 4% formaldehyde in
533 phosphate-buffered saline (PBS). To detect GGs, embryos were devitellinized using
534 heptane/methanol and subsequently washed three times in 1xPBS/0.1% Triton X-100. Embryos
535 were incubated first in 0.1M phosphatidic acid (pH 6) for 1hr and then in 0.15% periodic acid in
536 dH_2O for 15min. After one wash with dH_2O, embryos were incubated in Schiff's reagent (Sigma-
537 Aldrich) until the embryos went from uncolored, to pink, to red (~2 minutes). To stop the
538 reaction, it was quenched with 5.6% sodium borate/0.25 normal HCl stop solution for at least 2
539 minutes with agitation. After replacing half the volume of the stop solution with an equal

540 volume of 1×PBS/0.1% Triton X-100 to reintroduce detergent, the sample was shaken
541 vigorously to free embryos stuck to the container or each other. For subsequent imaging,
542 embryos were mounted in either Aqua-Poly/Mount, Polysciences, or glycerol (90% glycerol,
543 10% PBS). Mounts with 'antifade' or O_2 scavenging additives should be avoided. To determine
544 the specificity of the PAS signal, fixed and devitellinized embryos were first incubated with α-
545 amylase (Porcine, Sigma Aldrich, 0.2mg/mL in PBS, incubated for 2hrs) to specifically digest the
546 α-(1,4) glycosidic linkages in glycogen.

547 To detect LDs by staining, the methanol step needs to be omitted as it extracts neutral lipids.
548 Instead, embryos were washed extensively with 1×PBS/0.1% Triton X-100 to remove residual
549 heptane in a wire mesh basket then transferred to a 1.7mL microcentrifuge tube. They were
550 then washed 2x with 1×PBS/0.1% Triton X-100. If costaining with PAS, proceed to the
551 phosphatidic acid incubation step, adding 1µL of 1mg/mL BODIPY 493/503, Invitrogen, then
552 proceeding with subsequent steps as normal. Red lipid dyes overlap Schiff's reagent's spectra
553 and should be avoided for costaining.

554 For staining of lipid droplets without PAS costaining, remove the 1×PBS/0.1% Triton X-100
555 wash, and replace with 1×PBS/0.5% Triton X-100/10% BSA/0.02% sodium azide (toxic) and
556 incubate for 1 hr. Replace the solution with fresh 1×PBS/0.5% Triton X-100/10% BSA/0.02%
557 sodium azide and add either 1µL of 1mg/mL BODIPY 493/503 in DMSO, 1 µL LipidSpot 610
558 (1000x) (Biotium) in DMSO, or 10µL of 200mg/mL (Sigma Aldrich) in acetone.

559 To determine the distribution of LDs and GGs in centrifuged embryos, *in-vivo* centrifugation was
560 performed as described[20], followed by fixation and simultaneous LD/GG detection as above. For
561 analyzing follicles, ovaries were dissected from females maintained on yeast at 25°C overnight.
562 Samples were then fixed with 4% formaldehyde in PBS for 15 min, washed in 1xPBS/0.1%Triton
563 X-100, and simultaneously stained for LDs and GGs as above.

564

565 Live imaging

566 For live imaging involving dye injections, a previously published procedure was followed[14]. In
567 short, embryos were collected on apple juice plates for the desired time, hand-dechorionated,
568 transferred to a coverslip with heptane glue, desiccated, and placed in Halocarbon oil 700.
569 Embryos were then injected with BODIPY 493/503 (1mg/mL), LysoTracker Red (1mM) or
570 LipidSpot 610 (1000x) and imaged on a Leica Sp5 confocal microscope.

571 For live imaging of Glycogenin-YFP and YV autofluorescence, embryos were collected on apple
572 juice plates for the desired time, hand-dechorionated, transferred to a coverslip with heptane
573 glue, covered with Halocarbon oil 27, and imaged. To improve signal, flies were kept in the
574 dark, and light exposure during embryo preparation was kept to a minimum.

575

576 TEM

577 Embryos were collected from 7- to 14-day-old flies, dechorionated in 3% sodium hypochlorite,
578 and washed extensively with distilled water. Embryos were fixed in
579 4%paraformaldehyde/2%gluteradlehyde/PBS with an equal volume of heptane added. The vials

580 were shaken then left on an agitator for 20 minutes. After fixation, embryos were washed
581 extensively with 1×PBS/0.1% Triton X-100, then transferred onto a piece of double-sided tape,
582 adhered, then submerged with 1×PBS/0.1% Triton X-100. The embryos were then gently hand
583 rolled using fine forceps until the vitelline membrane was removed. Embryos were transferred
584 to a small glass vial. The embryos were then fixed a second time with
585 4%paraformaldehyde/2%gluteradlehyde/PBS, excluding the heptane, for 30 minutes. Embryos
586 were then washed three times with 0.2 M sucrose in 0.1M cacodylate buffer. They were
587 washed an additional 3 times in 0.1 M sodium cacodylate before post fixation in 1% osmium
588 tetroxide for 2 hours followed by uranyl acetate enhancement in 0.5% uranyl acetate overnight
589 at 4 °C. Specimen were washed and then dehydrated in a graded ethanol series, transitioned to
590 propylene oxide and embedded in an Epon/Araldite resin. Thin sections were stained with
591 0.3% lead citrate and imaged on a Hitachi 7650 transmission electron microscope using an 11
592 MP Gatan Erlanshen CCD camera. TEM work was conducted at the Electron and Cryo
593 Microscopy Resource in the Center for Advanced Research Technologies at the University of
594 Rochester.

595

596 Quantification of TEMs

597 To quantify the association of LDs and GGs, LDs were manually identified based on their
598 appearance and size (diameter of 0.3-0.75µm), while GGs were manually identified based on
599 the staining pattern and diameter (2-7µm). The two structures were labeled associated if the
600 distance between them was less than 30nm (~2pixels).

601

602 Particle Image Velocimetry

603 We performed PIV as described in[14]. The motion of acidic organelles and LDs was captured
604 simultaneously in the same embryos. Embryos were collected, staged, mounted on a coverslip,
605 and co-injected with BODIPY 493/503 and Lysotracker Red as described above. Per genotype,
606 three embryos were imaged at 25°C. Timeseries were captured by confocal microscopy at a
607 rate of 1 frame per 30 seconds, within a superficial plane of the embryo. The raw timeseries
608 were then analyzed, finding the 8th nuclear division by first finding the division where nuclei
609 arrive at the periphery (the 9th division), then going back one contraction cycle. 10 sequential
610 frames were taken from this division starting at the period of the highest lipid droplet motion
611 determined empirically. The signal from the embryos was then isolated from these 10 frames
612 using a mask. These processed frames were then fed into a PIV algorithm based on OpenPIV, a
613 python-based PIV implementation, generating 9 frame transitions per timeseries. The PIV
614 analysis script used is available as supplemental data from our previous publication [14]. The
615 output vectors for each transition were then processed to remove any vectors which failed to
616 meet or exceeded the empirically determined vector boundaries. Then directionality was
617 removed, the vectors were averaged across the transition, pixels were converted to microns,
618 and these averages were plotted on violin plots to show that pulses were being captured.

619 To perform PIV analysis for YVs, the same procedure was followed, with the exception that
620 embryos were not injected, and embryos were illuminated with a 405nm laser and yolk
621 autofluorescence was captured by collecting emission in a 410-500nm window.

622

623 Statistics

624 All statistics were done using Graphpad Prism. P values were calculated using 2-tailed, unpaired
625 Student's T-tests. At least 3 embryos were used per genotype. For the PIV statistical
626 comparisons 3 embryos were used per genotype contributing 9 transitions per embryo, thus n =
627 27, at least, per genotype.

628 The questions we sought to answer with statistical tests were "Are the Jabba LD:GG complexes
629 flowing slower then wild-type singular LDs?". Having received a positive result from this
630 question, we next asked "Is the flow generally slower in Jabba than wild-type or is the
631 diminished LD:GG speed due to complex formation?" for which we used acidic organelles and
632 YVs as unclustered controls. These are binary questions seeking to determine if two populations
633 of related numbers (flow speeds of organelles in each genotype) were different, thus we chose
634 to use Student's t-tests.

Acknowledgements

We thank the Blooming Drosophila Stock Center, the Kyoto Stock Center, and Ramona Lattao for fly stocks. We thank Zehra Ali-Murthy and Thomas Kornberg (University of California San Francisco) who provided us with the protocol for fPAS staining. TEM analysis was performed by Chad Galloway and Karen Bentley in the Electron Microscopy Shared Resource Laboratory at the University of Rochester Medical Center. We are grateful to Fredrick Gootkind for initial analysis of the LD clustering phenotype in *Jabba* mutants and Ethan Fisher for his work on fPAS staining. This work was supported by National Institutes of Health grants F31 HD100127 (to M. D. K.) and R01 GM102155 (to M. A. W).

Authorship contributions

M.D.K. conducted most of the experiments and analyzed the data, under guidance by M.A.W. M.D.K. and M.A.W. designed the overall project. M.R.J., J.M.T, and A.M. contributed experiments, technical advice, and conceptual discussions. M.R.J. performed initial analysis of GGs by fPAS staining and of GG-LD interactions in *Jabba* mutants. J.M.T. performed *in vivo* centrifugation experiments. A.M. performed initial electron microscopy characterization of *Jabba* mutants and advised on details and troubleshooting for the electron microscopy analysis included in the manuscript. M.D.K. and M.A.W. wrote the manuscript. All authors critically read the manuscript and provided feedback. M.D.K and M.A.W. contributed funding by National Institutes of Health grants F31 HD100127 (to M. D. K.) and R01 GM102155 (to M. A. W).

Competing interests

The authors declare no competing interests.

Materials and Correspondence

Correspondence and material requests should be addressed to Michael A. Welte.

References

1 Gandara, L. & Wappner, P. Metabo-Devo: A metabolic perspective of development. *Mech Dev* **154**, 12-23, doi:10.1016/j.mod.2018.02.004 (2018).

2 Tennessen, J. M. *et al.* Coordinated metabolic transitions during Drosophila embryogenesis and the onset of aerobic glycolysis. *G3 (Bethesda)* **4**, 839-850, doi:10.1534/g3.114.010652 (2014).

3 Song, Y. *et al.* Energy budget of Drosophila embryogenesis. *Curr Biol* **29**, R566-R567, doi:10.1016/j.cub.2019.05.025 (2019).

4 Miyazawa, H. & Aulehla, A. Revisiting the role of metabolism during development. *Development* **145**, doi:10.1242/dev.131110 (2018).

5 King, R. C. *Ovarian Development in Drosophila melanogaster*. (Academic Press 1970).

6 An, P. N., Yamaguchi, M., Bamba, T. & Fukusaki, E. Metabolome analysis of Drosophila melanogaster during embryogenesis. *PLoS One* **9**, e99519, doi:10.1371/journal.pone.0099519 (2014).

7 Gutzeit, H. O., Zissler, D., Grau, V., Liphardt, M. & Heinrich, U. R. Glycogen stores in mature ovarian follicles and young embryos of Drosophila: ultrastructural changes and some biochemical correlates. *Eur J Cell Biol* **63**, 52-60 (1994).

8 Jose A. Campos-Ortega, V. H. *The Embryonic Development of Drosophila Melanogaster*. (Springer-Verlag, 1985).

9 Reed, B. H., Wilk, R., Schock, F. & Lipshitz, H. D. Integrin-dependent apposition of Drosophila extraembryonic membranes promotes morphogenesis and prevents anoikis. *Curr Biol* **14**, 372-380, doi:10.1016/j.cub.2004.02.029 (2004).

10 Welte, M. A., Gross, S. P., Postner, M., Block, S. M. & Wieschaus, E. F. Developmental regulation of vesicle transport in Drosophila embryos: forces and kinetics. *Cell* **92**, 547-557, doi:10.1016/s0092-8674(00)80947-2 (1998).

11 Welte, M. A. As the fat flies: The dynamic lipid droplets of Drosophila embryos. *Bba-Mol Cell Biol L* **1851**, 1156-1185, doi:10.1016/j.bbalip.2015.04.002 (2015).

12 Deneke, V. E. *et al.* Self-Organized Nuclear Positioning Synchronizes the Cell Cycle in Drosophila Embryos. *Cell* **177**, 925-941 e917, doi:10.1016/j.cell.2019.03.007 (2019).

13 Victoria E. Foe, G. M. O., Bruce A. Edgar. in *The Development of Drosophila melanogaster* Vol. 1 (ed Alfonso Martinez Arias Michael Bate) (Cold Spring Harbor Laboratory Press, 1993).

14 Kilwein, M. D. & Welte, M. A. Visualizing Cytoskeleton-Dependent Trafficking of Lipid-Containing Organelles in Drosophila Embryos. *J Vis Exp*, doi:10.3791/63291 (2021).

15 Arora, G. K., Tran, S. L., Rizzo, N., Jain, A. & Welte, M. A. Temporal control of bidirectional lipid-droplet motion in Drosophila depends on the ratio of kinesin-1 and its co-factor Halo. *J Cell Sci* **129**, 1416-1428, doi:10.1242/jcs.183426 (2016).

16 Sieber, M. H., Thomsen, M. B. & Spradling, A. C. Electron Transport Chain Remodeling by GSK3 during Oogenesis Connects Nutrient State to Reproduction. *Cell* **164**, 420-432, doi:10.1016/j.cell.2015.12.020 (2016).

17 Prats, C., Graham, T. E. & Shearer, J. The dynamic life of the glycogen granule. *J Biol Chem* **293**, 7089-7098, doi:10.1074/jbc.R117.802843 (2018).

18 Lowe, N. *et al.* Analysis of the expression patterns, subcellular localisations and interaction partners of Drosophila proteins using a pigP protein trap library. *Development* **141**, 3994-4005, doi:10.1242/dev.111054 (2014).

19 Cermelli, S., Guo, Y., Gross, S. P. & Welte, M. A. The lipid-droplet proteome reveals that droplets are a protein-storage depot. *Curr Biol* **16**, 1783-1795, doi:10.1016/j.cub.2006.07.062 (2006).

20 Tran, S. L. & Welte, M. A. In-vivo centrifugation of Drosophila embryos. *J Vis Exp*, doi:10.3791/2005 (2010).

712 21 Rickoll, W. L. Cytoplasmic continuity between embryonic cells and the primitive yolk sac during
713 early gastrulation in Drosophila melanogaster. *Dev Biol* **49**, 304-310, doi:10.1016/0012-
714 1606(76)90278-5 (1976).
715 22 Li, Z. *et al.* Lipid droplets control the maternal histone supply of Drosophila embryos. *Curr Biol*
716 **22**, 2104-2113, doi:10.1016/j.cub.2012.09.018 (2012).
717 23 Lattao, R., Rangone, H., Llamazares, S. & Glover, D. M. Mauve/LYST limits fusion of lysosome-
718 related organelles and promotes centrosomal recruitment of microtubule nucleating proteins.
719 *Dev Cell* **56**, 1000-1013 e1006, doi:10.1016/j.devcel.2021.02.019 (2021).
720 24 Brewer, M. K. & Gentry, M. S. Brain Glycogen Structure and Its Associated Proteins: Past,
721 Present and Future. *Adv Neurobiol* **23**, 17-81, doi:10.1007/978-3-030-27480-1_2 (2019).
722 25 Froese, D. S. *et al.* Structural basis of glycogen branching enzyme deficiency and pharmacologic
723 rescue by rational peptide design. *Hum Mol Genet* **24**, 5667-5676, doi:10.1093/hmg/ddv280
724 (2015).
725 26 Mitchell A. Sullivan, F. V., Richard A. Cave, David Stapleton, Angus A. Gray-Weale, and Robert G.
726 Gilbert. Nature of α and β Particles in Glycogen Using Molecular Size Distributions.
727 *Biomacromolecules* doi:10.1021/bm100074p (2010).
728 27 Tan, X. *et al.* Proteomic Investigation of the Binding Agent between Liver Glycogen beta
729 Particles. *ACS Omega* **3**, 3640-3645, doi:10.1021/acsomega.8b00119 (2018).
730 28 Yamada, T. *et al.* The role of glycogen in development and adult fitness in Drosophila.
731 *Development* **146**, doi:10.1242/dev.176149 (2019).
732 29 Gross, S. P., Welte, M. A., Block, S. M. & Wieschaus, E. F. Dynein-mediated cargo transport in
733 vivo. A switch controls travel distance. *J Cell Biol* **148**, 945-956, doi:10.1083/jcb.148.5.945
734 (2000).
735 30 Shubeita, G. T. *et al.* Consequences of motor copy number on the intracellular transport of
736 kinesin-1-driven lipid droplets. *Cell* **135**, 1098-1107, doi:10.1016/j.cell.2008.10.021 (2008).
737 31 Kuhn, H., Sopko, R., Coughlin, M., Perrimon, N. & Mitchison, T. The Atg1-Tor pathway regulates
738 yolk catabolism in Drosophila embryos. *Development* **142**, 3869-3878, doi:10.1242/dev.125419
739 (2015).
740 32 Nguyen, T. B. *et al.* DGAT1-Dependent Lipid Droplet Biogenesis Protects Mitochondrial Function
741 during Starvation-Induced Autophagy. *Dev Cell* **42**, 9-21 e25, doi:10.1016/j.devcel.2017.06.003
742 (2017).
743 33 Chitraju, C. *et al.* Triglyceride Synthesis by DGAT1 Protects Adipocytes from Lipid-Induced ER
744 Stress during Lipolysis. *Cell Metab* **26**, 407-418 e403, doi:10.1016/j.cmet.2017.07.012 (2017).
745 34 Mashek, D. G., Li, L. O. & Coleman, R. A. Long-chain acyl-CoA synthetases and fatty acid
746 channeling. *Future Lipidol* **2**, 465-476, doi:10.2217/17460875.2.4.465 (2007).
747 35 Rambold, A. S., Cohen, S. & Lippincott-Schwartz, J. Fatty acid trafficking in starved cells:
748 regulation by lipid droplet lipolysis, autophagy, and mitochondrial fusion dynamics. *Dev Cell* **32**,
749 678-692, doi:10.1016/j.devcel.2015.01.029 (2015).
750 36 Herms, A. *et al.* AMPK activation promotes lipid droplet dispersion on detyrosinated
751 microtubules to increase mitochondrial fatty acid oxidation. *Nat Commun* **6**, 7176,
752 doi:10.1038/ncomms8176 (2015).
753 37 M.D., K. & M.A., W. Lipid droplet motility and organelle contacts. *Contact (Thousand Oaks)*
754 (2019).
755 38 Dutta, A. & Kumar Sinha, D. Turnover of the actomyosin complex in zebrafish embryos directs
756 geometric remodelling and the recruitment of lipid droplets. *Sci Rep* **5**, 13915,
757 doi:10.1038/srep13915 (2015).

758 39 Gupta, P., Martin, R., Knolker, H. J., Nihalani, D. & Kumar Sinha, D. Myosin-1 inhibition by PClP
759 affects membrane shape, cortical actin distribution and lipid droplet dynamics in early Zebrafish
760 embryos. *PLoS One* **12**, e0180301, doi:10.1371/journal.pone.0180301 (2017).
761 40 Welte, M. A. Expanding roles for lipid droplets. *Curr Biol* **25**, R470-481,
762 doi:10.1016/j.cub.2015.04.004 (2015).
763 41 Walther, T. C. & Farese, R. V., Jr. Lipid droplets and cellular lipid metabolism. *Annu Rev Biochem*
764 **81**, 687-714, doi:10.1146/annurev-biochem-061009-102430 (2012).

765
766

767 **Supplementary Figures**

768

769 Supplementary Figure 1. GG detection in in-vivo centrifuged syncytial embryos. A, A')
770 Glycogenin-YFP expressing embryo. A = bright field image; expected location of organelles
771 indicated on the left, according to [19] and this study. The least dense fraction (the refractive lipid
772 droplet cap) is at the top; the densest fractions (i.e., the refractive yolk vesicles and clear
773 glycogen) are at the bottom. Scale bar = 50 µm. A' = merged fluorescent image of the same
774 embryo showing Glycogenin-YFP (yellow) at the very bottom and YV autofluorescence (blue) in
775 the layer above). B,C) Centrifuged wild-type (B) and *Jabba* mutant (C) embryos and stained for
776 glycogen (fPAS, red) and LDs (BODIPY, cyan). In the wild type, glycogen and LDs are present at
777 opposite poles. In the *Jabba* embryo, LD and glycogen are co-mingled.

778

779 Supplementary Figure 2. Glycogen distribution at various embryonic stages. A) Glycogenin-YFP
780 at different stages showing the clustering of glycogen granules and exclusion of glycogen from
781 the pole plasm/pole cells (arrowhead). Left: YFP channel; right: corresponding brightfield
782 image. B, C) fPAS staining of wild-type embryos. B) At the onset of germ band extension, fPAS
783 signal is dimming and predominantly present the yolk cell. C) At the end of germ band
784 extension (>7 hrs post fertilization), fPAS staining is undetectable. D) Glycogenin-YFP embryo
785 during dorsal closure (~12 hours post fertilization). YFP signal is very faint and present in the
786 yolk cell. Signal appears brighter at the periphery due to optical sectioning. Images taken by
787 confocal microscopy. E) Time course of fPAS staining in wild-type and *Jabba* embryos imaged
788 using epifluorescence. The middle panels are at later germ band extension like that shown in
789 panel C. We notice no differences between the genotypes. All scale bars = 100 µm.
790

791 Supplementary Figure 3. A,B) TEM images of newly laid wild-type (A) and *Jabba* mutant (B)
792 embryos. GGs pseudo colored red; lipid droplets pseudo colored green. Scale bars = 2 µm. C)
793 Embryos of different genotypes stained for LDs (BODIPY493/503, cyan) and glycogen (fPAS). In
794 *Stur, klar, and LSD2/dPLIN2* null embryos, LDs are not associated with GGs. An embryo with
795 reduced *Jabba* dosage displays partial association. D) Live imaging of stage 2 wild-type and
796 *Jabba* embryos injected with BODIPY493/503 (cyan) to track LD motion. Arrowheads track
797 selected LDs through time. The direction of the cytoplasmic flow is indicated by the black
798 arrow. E) Stage 2 wild-type and *Jabba* embryos injected with LipidSpot 610 to label LDs
799 (magenta)and co-imaged for YV autofluorescence (blue). In the *Jabba* embryo, the LDs rings are
800 not around YVs. C-E) Scale bars = 10 µm; images recorded by confocal microscopy. F) cartoon
801 showing the gross directions of the flowing cytoplasm during stages 1-3.
802

803 Supplementary Figure 4. Jabba prevents inappropriate interaction between LDs and GGs. A)
804 TEM cross section of < 1hr old wild-type embryo. B) TEM cross section of a < 1-hour old *Jabba*
805 embryo, note the LDs bound to GG and the lack of LDs free in the cytoplasm. Scale bars = 20
806 µm.
807

808 **Videos**
809
810 Supplementary Video 1. Wild-type embryo injected with BODIPY493/503 (displayed in inverted
811 greyscale) to label LDs. The embryo is imaged in a subcortical plane. The video starts in stage 1-
812 2 (<1 hour post fertilization) and captures 30 minutes real time. Scale bar is 100 µm.
813
814 Supplementary Video 2. Wild-type embryo injected with BODIPY 493/503 to label LDs (shown in
815 greyscale). The embryo is imaged at 40 µm below the subcortical plane. The video captures
816 about 90minutes real time. Scale bar is 100 µm.
817
818 Supplementary Video 3. Glycogenin-YFP embryo with YFP in greyscale. The embryo is imaged in
819 a subcortical plane. The video starts in stage 1-2 and captures 20 minutes real time. Scale bar is
820 100 µm.
821
822 Supplementary Video 4. Glycogenin-YFP embryo with YFP in greyscale. The embryo is imaged in
823 a subcortical plane. The video starts in stage 1-2 (<1 hour post fertilization) and captures 2
824 hours real time. Scale bar is 100 µm.
825
826 Supplementary Video 5. Jabba embryo injected with BODIPY 493/503 (displayed in inverted
827 greyscale) to label LDs. The embryo is imaged in a subcortical plane. The video starts in stage 1-
828 2 (<1 hour post fertilization) and captures 30 minutes real time. Scale bar is 100 µm.
829
830 Supplementary Video 6. Jabba embryo injected with BODIPY 493/503 to label LDs (shown in
831 greyscale). The embryo is imaged at 40 µm below the subcortical plane. The video captures
832 about2 hours real time. Scale bar is 100 µm.